Article

Cell Stem Cell

Tracing the skeletal progenitor transition during postnatal bone formation

Graphical Abstract

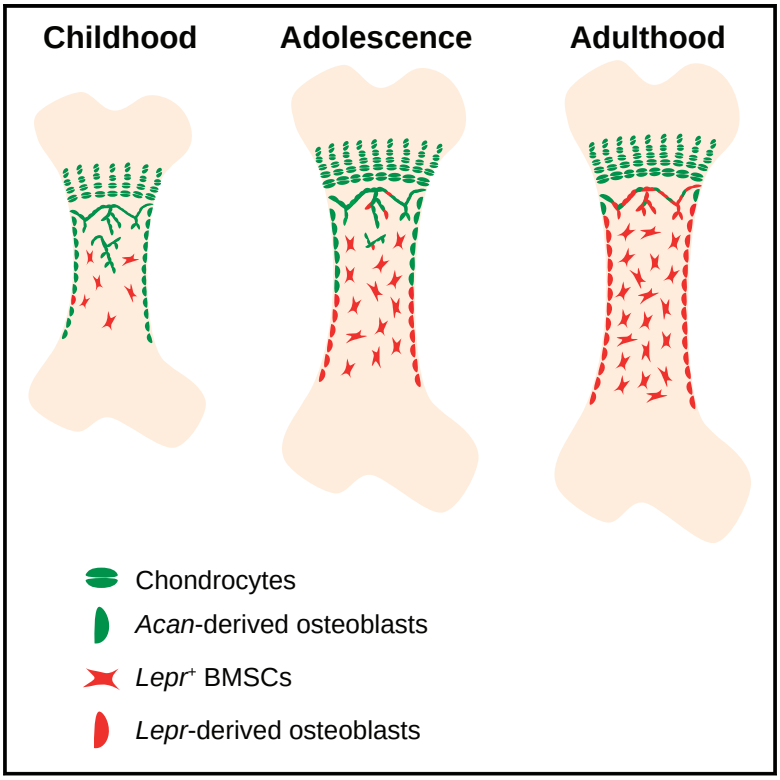

Authors

Hui Sophie Shu, Yiming Liam Liu, Xinyu Thomas Tang, Xinyi Shirley Zhang, Bin Zhou, Weiguo Zou, Bo O. Zhou

Correspondence

bo.zhou@sibcb.ac.cn

In brief

Shu et al. discovered that bone formation before and after adolescence is dominated sequentially by chondrocytes and *Lepr*$^{+}$ BMSCs. They regulate bone lengthening and thickening, respectively. This transition explains, from a stem cell perspective, how mammalian limb bones transition from rapid longitudinal growth to slower appositional remodeling after adolescence.

Highlights

- Bone formation before and after adolescence is controlled by distinct progenitors
- Chondrocytes and *Lepr*$^{+}$ BMSCs mediate bone lengthening and thickening, respectively
- The adult skeletal progenitors derive mainly from developmental skeletal progenitors
- Running enhances osteogenesis by developmental but not adult skeletal progenitors

Shu et al., 2021, Cell Stem Cell *28*, 2122–2136
December 2, 2021
https://doi.org/10.1016/j.stem.2021.08.010

CellPress

CellPress

Cell Stem Cell

Article

Tracing the skeletal progenitor transition during postnatal bone formation

Hui Sophie Shu,[1,3] Yiming Liam Liu,[1,3] Xinyu Thomas Tang,[1] Xinyi Shirley Zhang,[1] Bin Zhou,[1] Weiguo Zou,[1] and Bo O. Zhou[1,2,4,*]

[1]State Key Laboratory of Cell Biology, Shanghai Institute of Biochemistry and Cell Biology, Center for Excellence in Molecular Cell Science, Chinese Academy of Sciences, University of Chinese Academy of Sciences, Shanghai 200031, China

[2]State Key Laboratory of Experimental Hematology, Institute of Hematology & Blood Diseases Hospital, Chinese Academy of Medical Sciences, Tianjin 300020, China

[3]These authors contributed equally

[4]Lead contact

*Correspondence: bo.zhou@sibcb.ac.cn

https://doi.org/10.1016/j.stem.2021.08.010

SUMMARY

Multiple distinct types of skeletal progenitors have been shown to contribute to endochondral bone development and maintenance. However, the division of labor and hierarchical relationship between different progenitor populations remain undetermined. Here we developed dual-recombinase fate-mapping systems to capture the skeletal progenitor transition during postnatal bone formation. We showed that postnatal osteoblasts arose primarily from chondrocytes before adolescence and from *Lepr*$^+$ bone marrow stromal cells (BMSCs) after adolescence. This transition occurred in the diaphysis during adolescence and progressively spread to the metaphysis. The osteoblast-forming *Lepr*$^+$ BMSCs derived primarily from fetal *Col2*$^+$ cells. Conditional deletion of *Runx2* from perinatal chondrocytes and adult *Lepr*$^+$ BMSCs impaired bone lengthening and thickening, respectively. Forced running increased osteoblast formation by perinatal chondrocytes but not by adult *Lepr*$^+$ BMSCs. Thus, the short-term developmental skeletal progenitors generated the long-term adult skeletal progenitors. They sequentially control the growth and maintenance of endochondral bones.

INTRODUCTION

Development, maintenance, and regeneration of bones require continuous osteoblast formation by skeletal progenitors (Ono et al., 2019). Skeletal progenitors have been identified in multiple cell types of the endochondral bones in the mouse, including various subsets of bone marrow stromal cells (Méndez-Ferrer et al., 2010; Mizoguchi et al., 2014; Park et al., 2012; Pineault et al., 2019; Rux et al., 2016; Seike et al., 2018; Worthley et al., 2015; Zhou et al., 2014a), chondrocytes (Mizuhashi et al., 2018; Ono et al., 2014; Yang et al., 2014b; Zhou et al., 2014b), and periosteal stromal cells (Debnath et al., 2018; Duchamp de Lageneste et al., 2018; Ortinau et al., 2019).

Single-cell RNA sequencing has defined bone marrow stromal cells (BMSCs) as Leptin receptor (LepR)-expressing BMSCs that abundantly expressed hematopoietic niche factors (Baryawno et al., 2019; Tikhonova et al., 2019). LepR$^+$ BMSCs contain virtually all colony-forming unit-fibroblasts (CFU-Fs) in the bone marrow (Zhou et al., 2014a). Fate mapping with *Lepr*-Cre labeled most osteoblasts and adipocytes in adult bone marrow (Mizoguchi et al., 2014; Zhou et al., 2014a). Thus, LepR$^+$ BMSCs may represent the main skeletal progenitor population in adult bone marrow, but the lack of a *Lepr-creER* allele from which fate mapping could be initiated during adulthood raises the possibility that early postnatal progeny of LepR$^+$ cells may be the key source of osteoblasts during adulthood. It is also uncertain whether LepR$^+$ BMSCs are self-renewable or whether they are replenished continuously by LepR$^-$ progenitors during adulthood.

In the endochondral ossification model, cartilage does not form bone but, rather, serves as a template that is replaced by new bone. Recent studies have challenged this dogma by showing that early postnatal cells marked by *Col2*-CreER, *Sox9*-CreER, *Acan*-CreER, or *Col10*-Cre contribute to endochondral bones that persist throughout adulthood (Ono et al., 2014; Yang et al., 2014a, 2014b; Zhou et al., 2014b). The relative contributions of chondrocytes and BMSCs to bone formation at different stages have not been determined.

BMSCs have been thought to originate from fetal Osterix (Osx)$^+$ perichondral precursors that invade the cartilage template along with the blood vessels (Maes et al., 2010). Recent evidence has suggested that chondrocytes give rise to a significant portion of BMSCs that persist in adulthood (Ono et al., 2014). This raises the possibility that the BMSCs maintaining adult bones arise from chondrocytes. However, this idea is difficult to address using single-recombinase fate-mapping systems, such as *Col2*-Cre or *Acan*-CreER, because it is hard

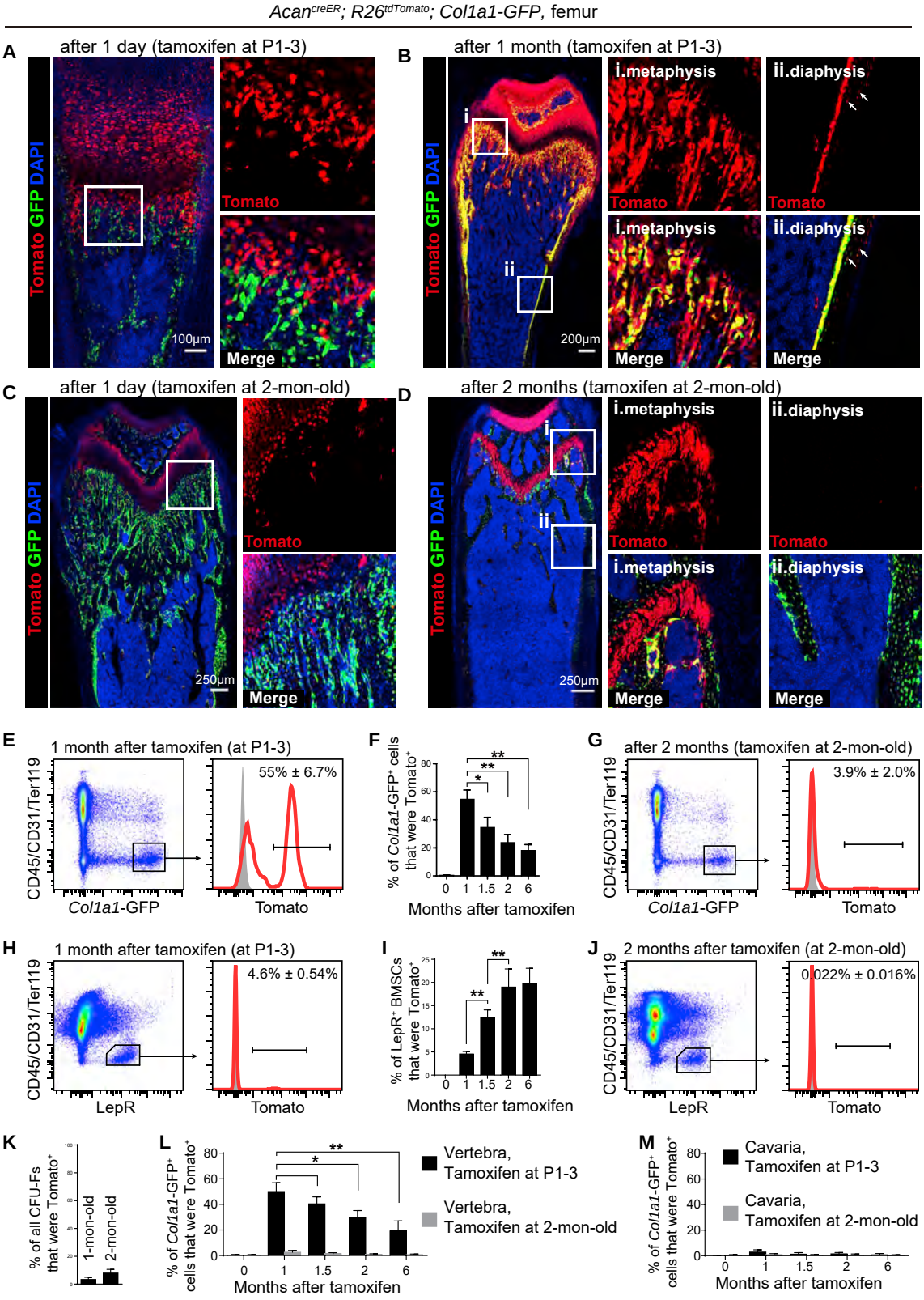

Figure 1. Chondrocytes form most osteoblasts in early postnatal bones, but their contribution declines by 2 months of age

(A and B) Confocal imaging of femur sections from *Acan*^{creER}*; R26*^{tdTomato}*; Col1a1-GFP* mice that had been tamoxifen treated at P1–P3. Mice were analyzed at 1 day (A) and 1 month after the treatment (B). Arrows indicate Tomato$^+$ osteocytes. n = 3 mice per condition from 3 independent experiments.

(legend continued on next page)

to distinguish whether the undifferentiated BMSCs that arise from these cell populations form osteoblasts independent of the osteoblasts formed by the chondrocytes themselves. In this study, we generated a series of single-recombinase and dual-recombinase fate-mapping systems to trace chondrocytes and *Lepr*$^{+}$ BMSCs, comparing their contributions to osteogenesis during bone growth and maintenance and elaborating their relationship.

RESULTS

Perinatal chondrocytes form most of the new osteoblasts by 1 month of age

To determine the contribution of chondrocytes to postnatal bone formation, we crossed *Acan*^{creER} knockin mice (Henry et al., 2009) with *Rosa26*$^{CAG\text{-}loxp\text{-}STOP\text{-}loxp\text{-}tdTomato}$ (*R26*^{tdTomato}) knockin mice (Madisen et al., 2010) and *Col1a1*2.3-GFP* (*Col1a1-GFP*) transgenic mice (Kalajzic et al., 2002) to generate *Acan*^{creER}*; R26*^{tdTomato}*; Col1a1-GFP* mice. *Acan* (*Aggrecan*) promoter-driven Cre expression did not show any leakiness in the bone marrow without tamoxifen treatment (Figure S1A). We administered tamoxifen to these mice from post-natal day 1 (P1)–P3. At P2 and P3, Tomato expression was highly restricted to the growth plate (Figures S1B and S1C). At P4, Tomato^{+} non-chondrocytes appeared underneath the growth plate (Figures 1A and S1D); however, they were negative for aggrecan expression (Figure S1E), suggesting that they are not *Acan*$^{+}$ cells but progeny of *Acan*$^{+}$ cells. Sox9^{+} columnar chondrocytes and Col10^{+} hypertrophic chondrocytes were marked by Tomato (Figures S1F and S1G). *Col1a1*-GFP^{+} osteoblasts were uniformly Tomato^{-} at this stage (Figures 1A and 1F). 1 month after tamoxifen treatment, Tomato^{+} stromal cells were distributed throughout the bone marrow (Figures 1B and S1N). Osteoblasts, as revealed by *Col1a1*-GFP (Figure 1B) or anti-Runx2 staining (Figure S1H), were co-labeled extensively by Tomato at the metaphysis and diaphysis. A significant portion of osteocytes, as revealed by anti-sclerostin staining, were also marked by Tomato in 1-month-old mice (Figures 1B, arrows, and S1I). Flow cytometry analysis of enzymatically dissociated femora showed that 55% ± 6.7% of all *Col1a1*-GFP^{+} osteoblasts expressed Tomato (Figure 1E), suggesting that perinatal chondrocytes are the major contributors to osteoblast production by 1 month of age.

The contribution of chondrocytes to osteoblasts decreases by adulthood

2 months after tamoxifen treatment, we still observed many Tomato^{+} osteoblasts in the metaphysis of *Acan*^{creER}*; R26*^{tdTomato}*; Col1a1-GFP* mice pulsed at P1–P3 (Figure S1M), but there were considerably fewer in the diaphysis (compare Figures 1Bii and S1Mii). By flow cytometry, only 24% ± 6.0% of all *Col1a1*-GFP^{+} osteoblasts expressed Tomato in these mice, significantly less than that at 1 month of age (Figure 1F). This value decreased further to 18% ± 4.4% 6 months after tamoxifen treatment (Figure 1F). These data suggested that the contribution of perinatal chondrocytes to osteoblast formation decreased progressively with age.

To determine whether adult chondrocytes form osteoblasts, we administered tamoxifen to 2-month-old *Acan*^{creER}*; R26*^{tdTomato}*; Col1a1-GFP* mice. 1 day after tamoxifen treatment, we observed efficient and specific labeling of chondrocytes in the growth plate (Figures 1C and S1J–S1L). Unlike perinatal chondrocytes, 2-month-old chondrocytes generated few Tomato^{+} BMSCs (Figures 1D and S1N). Tomato^{+} osteoblasts were observed but restricted to metaphyseal regions adjacent to the growth plate (Figure 1D). By flow cytometry, only 3.9% ± 2.0% of all *Col1a1*-GFP^{+} osteoblasts expressed Tomato in these mice (Figure 1G). 6 months after tamoxifen treatment, we observed even fewer Tomato^{+} *Col1a1*-GFP^{+} osteoblasts (Figure S1O). Thus, adult chondrocytes generate only a few osteoblasts underneath the growth plate.

We determined the contribution of perinatal chondrocytes to LepR^{+} BMSCs. By flow cytometry, only 4.6% ± 0.54% of all LepR^{+} BMSCs expressed Tomato in 1-month-old *Acan*^{creER}*; R26*^{tdTomato}*; Col1a1-GFP* mice pulsed at P1–P3 (Figure 1H). This value increased gradually to 20% ± 3.3% by 2 months of age (Figure 1I). Approximately 3% and 8% of all CFU-Fs in the bone marrow expressed Tomato in 1- and 2-month-old mice, respectively (Figure 1K). 0.022% ± 0.016% of all LepR^{+} BMSCs expressed Tomato in 4-month-old *Acan*^{creER}*; R26*^{tdTomato}*; Col1a1-GFP* mice pulsed at 2 months of age (Figure 1J). These data suggest that perinatal chondrocytes generate a small subset of adult LepR^{+} BMSCs.

In vertebrae, which are also formed by endochondral ossification, we found that chondrocytes in *Acan*^{creER}*; R26*^{tdTomato}*; Col1a1-GFP* mice formed most osteoblasts before adolescence but few afterward (Figures 1L, S2A–S2C, S2F, and S2G),

(C and D) Confocal imaging of femur sections from *Acan*^{creER}*; R26*^{tdTomato}*; Col1a1-GFP* mice that had been tamoxifen treated at 2 months of age. Mice were analyzed at 1 day (C) and 2 months after the treatment (D). n = 3 mice per condition from 3 independent experiments.

(E and H) Flow cytometry analysis of enzymatically dissociated femur shafts (E) or bone marrow cells (H) from 1-month-old *Acan*^{creER}*; R26*^{tdTomato}*; Col1a1-GFP* mice that had been tamoxifen treated at P1–P3. Femora from *Col1a1-GFP* mice were set as negative controls (gray peak). n = 5 mice from 3 independent experiments.

(F and I) Quantification of the percentage of *Col1a1*-GFP^{+} osteoblasts (F) or LepR^{+} BMSCs (I) that were Tomato^{+} in *Acan*^{creER}*; R26*^{tdTomato}*; Col1a1-GFP* mice that had been tamoxifen treated at P1–P3 by flow cytometry. All data represent mean ± SD of 5 mice per time point from 5 independent experiments. The statistical significance of differences between different time points after tamoxifen was measured by repeated-measures one-way ANOVAs with Greenhouse-Geisser correction and Tukey's multiple comparisons tests (*$p < 0.05$, **$p < 0.01$).

(G and J) Flow cytometry analysis of enzymatically dissociated femur shafts (G) or bone marrow cells (J) from 4-month-old *Acan*^{creER}*; R26*^{tdTomato}*; Col1a1-GFP* mice that had been tamoxifen treated 2 months before. n = 3 mice from 3 independent experiments.

(K) Percentage of all CFU-F colonies from the femoral bone marrow of 1-month-old and 2-month-old *Acan*^{creER}*; R26*^{tdTomato} mice that expressed Tomato. Mice were tamoxifen treated at P1–P3. n = 5 mice from 3 independent experiments.

(L and M) Percentages of *Col1a1*-GFP^{+} osteoblasts that were Tomato^{+} in vertebrae (L) and calvaria (M) from *Acan*^{creER}*; R26*^{tdTomato}*; Col1a1-GFP* mice. Data were measured by flow cytometry. All data represent mean ± SD of 5 mice per time point from 3 independent experiments.

See also Figures S1 and S2.

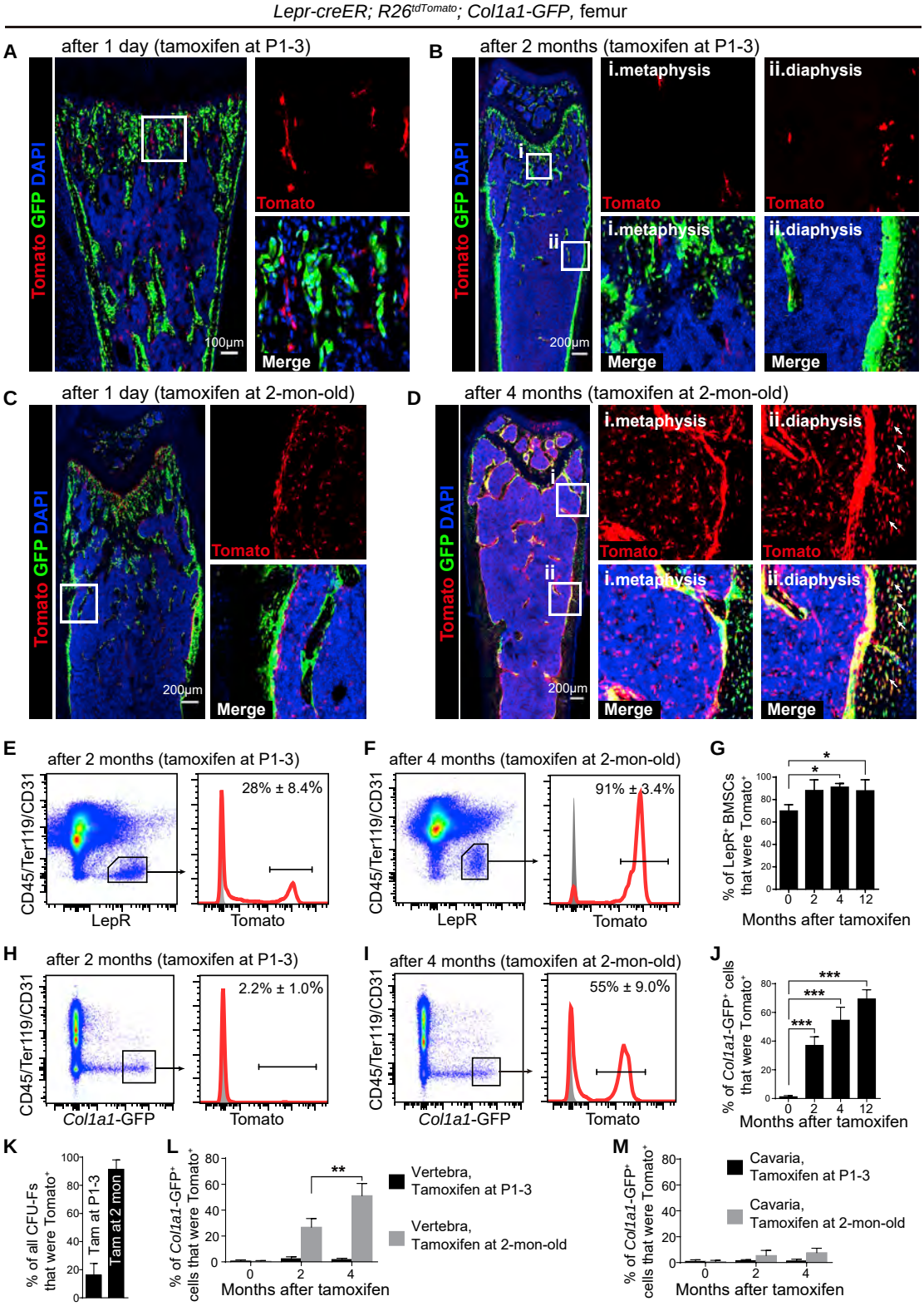

Figure 2. *Lepr*+ BMSCs form most osteoblasts during adulthood but few during development

(A and B) Confocal imaging of femur sections from *Lepr-creER; R26*^{tdTomato}*; Col1a1-GFP* mice that had been tamoxifen treated at P1–P3. Mice were analyzed 1 day (A) or 2 months (B) after the treatment. n = 3 mice per condition from 3 independent experiments.

(legend continued on next page)

consistent with our observations in the femur. In calvaria, whose formation involves intramembranous ossification, we detected few Tomato$^+$ stromal cells or osteoblasts in *Acan^{creER}; R26^{tdTomato}; Col1a1-GFP* mice, regardless of whether tamoxifen was administered at P1–P3 or 2 months of age (Figures 1M, S2D, S2E, S2H, and S2I), suggesting that postnatal chondrocytes are not the origin of osteoblasts in calvaria.

Perinatal *Lepr*$^+$ BMSCs rarely form osteoblasts

To determine the contribution of LepR$^+$ BMSCs to postnatal bone formation, we generated *Lepr-creER* BAC (bacterial artificial chromosome)-transgenic mice. These mice were crossed with *R26^{tdTomato}* and *Col1a1-GFP* mice to generate *Lepr-creER; R26^{tdTomato}; Col1a1-GFP* mice. *Lepr* promoter-driven Cre expression did not show any leakiness in the bone marrow without tamoxifen treatment (Figure S3A). At 1 day after tamoxifen treatment at P1–P3, a few Tomato$^+$ stromal cells appeared in the bone marrow (Figures 2A and S3B). 2 months after tamoxifen treatment, more Tomato$^+$ stromal cells were detected in the bone marrow (Figure 2B). By flow cytometry, they accounted for 28% ± 8.4% of all LepR$^+$ BMSCs in 2-month-old bone marrow (Figure 2E). This number decreased to 13% ± 4.2% 4 months after tamoxifen treatment (Figure S3C). On femur sections 2 months after tamoxifen treatment, most of the *Col1a1*-GFP$^+$ osteoblasts were Tomato negative (Figure 2B). Consistent with this, only 2.2% ± 1.0% of all *Col1a1*-GFP$^+$ osteoblasts were Tomato$^+$ by flow cytometry (Figure 2H). Thus, perinatal *Lepr*$^+$ cells make a limited and declining contribution to BMSCs and contribute minimally to bone formation in postnatal bone marrow.

Adult *Lepr*$^+$ BMSCs become the main source of new osteoblasts

We examined the Tomato expression pattern in *Lepr-creER; R26^{tdTomato}; Col1a1-GFP* mice 1 day after tamoxifen treatment at 2 months of age. Tomato expression was detected in stromal cells throughout the bone marrow (Figure S3F), accounting for 70% ± 5.6% of all *Lepr*$^+$ BMSCs (Figure 2G). Tomato expression was not detected in *Col1a1*-GFP$^+$ osteoblasts (Figures 2C and S3D; Video S1), VE-cadherin$^+$ endothelial cells (Figure S3E), aggrecan$^+$ chondrocytes (Figure S3G), and perilipin$^+$ adipocytes (Figure S3H). Thus, *Lepr*-CreER efficiently and specifically marks LepR$^+$ BMSCs in 2-month-old mice.

After 4 months of tracing, 91% ± 3.4% of all LepR$^+$ BMSCs were Tomato$^+$ in the femora of *Lepr-creER; R26^{tdTomato}; Col1a1-GFP* mice (Figures 2F and 2G). Virtually all Tomato$^+$ stromal cells were LepR$^+$ (Figures S3I and S3L). Similarly, 85% ± 4.5% of all PDGFRα^+ BMSCs were Tomato$^+$ (Figure S3J), and virtually all Tomato$^+$ stromal cells expressed PDGFRα (Figure S3K). Among all CFU-F colonies formed by whole bone marrow cells, 91% ± 6.7% of them expressed Tomato (Figure 2K). Consistent with this, fluorescence-activated cell sorting (FACS) of CD45$^-$Ter119$^-$CD31$^-$Lepr$^+$ cells recovered ~95% and ~85% of all CFU-Fs from the bone marrow and femur shaft, respectively. The percentage of LepR$^+$ BMSCs that were labeled by Tomato did not decrease even after tracing for 12 months (Figure 2G). Similarly, when tamoxifen was administered to these mice at 6 months of age, we found that LepR$^+$ BMSCs essentially overlapped with the Tomato$^+$ BMSCs at 8 months of age (Figures S3O and S3Q). Thus, unlike perinatal *Lepr*$^+$ cells, adult *Lepr*$^+$ BMSCs sustain themselves throughout adulthood.

In femur sections from 6-month-old *Lepr-creER; R26^{tdTomato}; Col1a1-GFP* mice that were treated with tamoxifen at 2 months of age, most *Col1a1*-GFP$^+$ osteoblasts in the femur, especially those in the diaphysis, were co-labeled by Tomato (Figure 2D). Tomato expression was also detected robustly in osteocytes in the bone (Figures 2D, arrows, and S3N). By flow cytometry, Tomato$^+$ cells accounted for 55% ± 9.0% of all *Col1a1*-GFP$^+$ osteoblasts in the femur (Figure 2I). This value increased to 69% ± 6.3% 12 months after tamoxifen treatment (Figure 2J). When these mice were treated with tamoxifen at 6 months of age, we detected that 36% ± 5.1% and 47% ± 8.0% of osteoblasts expressed Tomato at 8 and 10 months of age, respectively (Figure S3P). These data suggested that most of the newly formed osteoblasts during adulthood arise from adult *Lepr*$^+$ BMSCs.

In vertebrae, we found that adult but not perinatal *Lepr*$^+$ BMSCs from *Lepr-creER; R26^{tdTomato}; Col1a1-GFP* mice made a major contribution to bone formation (Figures 2L, S4A–S4C, S4F, and S4G), consistent with our observations in

(C and D) Confocal imaging of femur sections from *Lepr-creER; R26^{tdTomato}; Col1a1-GFP* mice that had been tamoxifen treated at 2 months of age. Mice were analyzed 1 day (C) and 4 months (D) after the treatment. Arrows indicate Tomato$^+$ osteocytes. n = 3 mice per condition from 3 independent experiments.

(E and F) Flow cytometry analysis of enzymatically dissociated bone marrow cells from 2-month-old *Lepr-creER; R26^{tdTomato}; Col1a1-GFP* mice that had been tamoxifen treated at P1–P3 (E) or from 6-month-old *Lepr-creER; R26^{tdTomato}; Col1a1-GFP* mice that had been tamoxifen treated at 2 months of age (F). Bone marrow cells from wild-type mice were set as negative controls (gray peak). n = 5 mice per condition from 5 independent experiments.

(G) Quantification of the percentage of all *Lepr*$^+$ BMSCs that were Tomato$^+$ in *Lepr-creER; R26^{tdTomato}; Col1a1-GFP* mice that had been tamoxifen treated at 2 months of age by flow cytometry. All data represent mean ± SD of 5 mice per time point from 5 independent experiments. The statistical significance of differences between different time points after tamoxifen was measured by repeated-measures one-way ANOVAs with Greenhouse-Geisser correction and Tukey's multiple comparisons tests (*$p < 0.05$).

(H and I) Flow cytometry analysis of enzymatically dissociated femora from 2-month-old *Lepr-creER; R26^{tdTomato}; Col1a1-GFP* mice that had been tamoxifen treated at P1–P3 (H) or from 6-month-old *Lepr-creER; R26^{tdTomato}; Col1a1-GFP* mice that had been tamoxifen treated at 2 months of age (I). Femora from *Col1a1-GFP* mice were set as negative controls (gray peak). n = 5 mice per condition from 5 independent experiments.

(J) Quantification of the percentage of *Col1a1*-GFP$^+$ osteoblasts that were Tomato$^+$ in *Lepr-creER; R26^{tdTomato}; Col1a1-GFP* mice that had been tamoxifen treated at 2 months of age by flow cytometry. All data represent mean ± SD of 5 mice per time point from 5 independent experiments. The statistical significance of differences between different time points after tamoxifen was measured by repeated-measures one-way ANOVAs with Greenhouse-Geisser correction and Tukey's multiple comparisons tests (***$p < 0.001$).

(K) Percentage of all CFU-F colonies from the femoral bone marrow of *Lepr-creER; R26^{tdTomato}* mice that expressed Tomato. Mice were analyzed 2 months after tamoxifen treatment. n = 5 mice from 3 independent experiments.

(L and M) Percentages of *Col1a1*-GFP$^+$ osteoblasts that were Tomato$^+$ in the vertebra (L) and calvaria (M) from *Lepr-creER; R26^{tdTomato}; Col1a1-GFP* mice. Data were measured by flow cytometry. All data represent mean ± SD of 5 mice per time point from 3 independent experiments.

See also Figures S3 and S4 and Video S1.

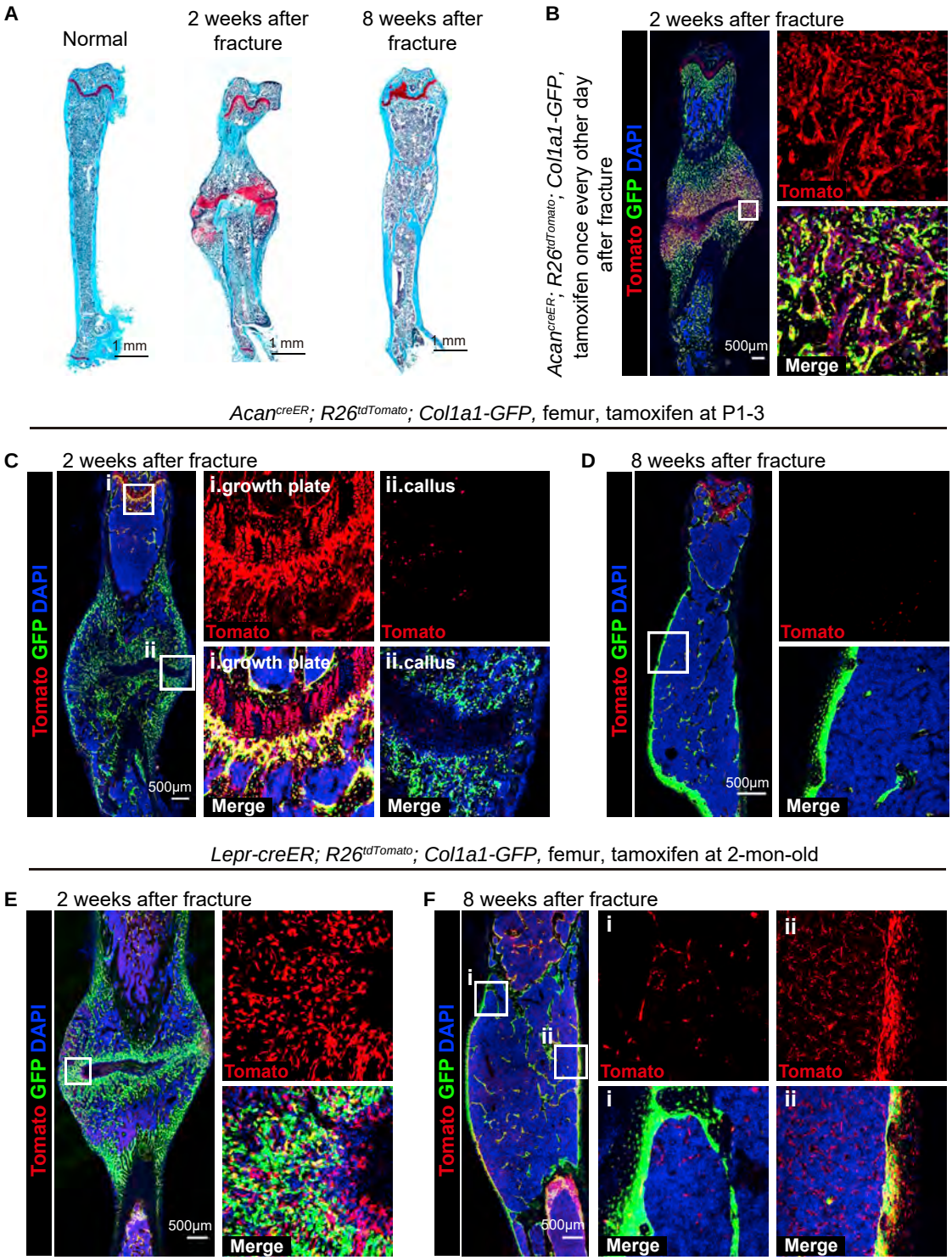

Figure 3. Adult *Lepr*$^{+}$ BMSCs, but not perinatal chondrocytes, contribute to fracture healing

(A) Safranin O staining of femur sections from normal mice or mice 2 or 8 weeks after fracture. n = 3 mice per condition from 3 independent experiments.

(B–D) Confocal imaging of femur sections from *Acan*^{creER}; *R26*^{tdTomato}; *Col1a1-GFP* mice 2 weeks (B and C) or 8 weeks (D) after fracture. Mice were tamoxifen-treated after fracture (B) or at P1–P3 (C and D). n = 3 mice per condition from 3 independent experiments.

(E and F) Confocal imaging of femur sections from *Lepr-creER; R26*^{tdTomato}; *Col1a1-GFP* mice 2 weeks (E) or 8 weeks (F) after fracture. Mice were tamoxifen-treated 2 months of age and fractured at 4 months of age. n = 3 mice per condition from 3 independent experiments.

See also Figure S5.

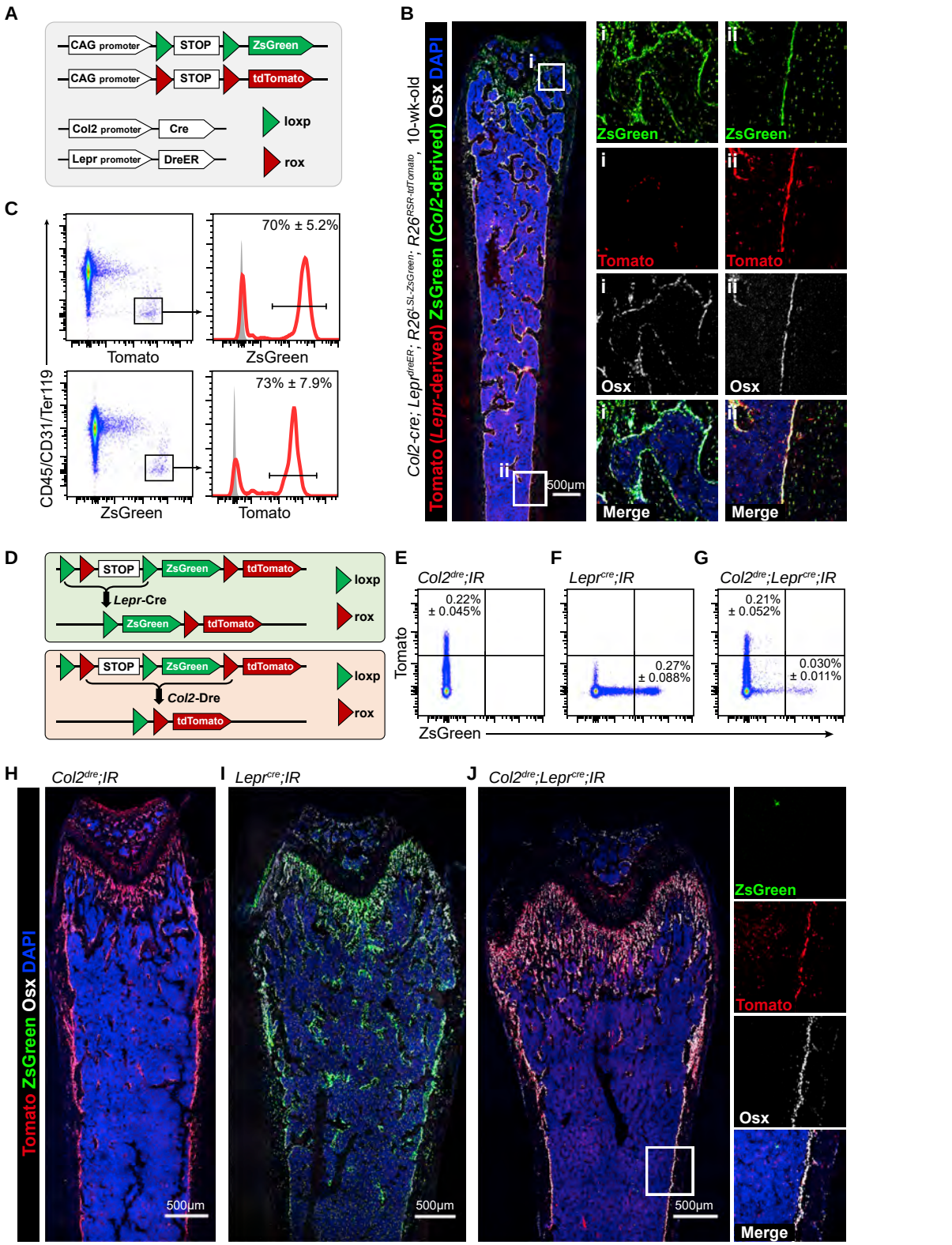

(legend on next page)

femora. In calvaria, although we detected robust Tomato expression in adult BMSCs, they formed a minor portion of osteoblasts (Figures 2M, S4D, S4E, S4H, and S4I), suggesting that *Lepr*$^{+}$ BMSCs are not the origin of osteoblasts in postnatal calvaria.

Most of the perilipin^{+} adipocytes expressed Tomato in the bone marrow from 6- and 14-month-old *Lepr-creER; R26*^{tdTomato} mice pulsed at 2 months of age (Figures S5A and S5C). At 2 weeks after lethal irradiation and bone marrow transplantation, adipocytes were increased markedly in the bone marrow of *Lepr-creER; R26*^{tdTomato} mice compared with non-irradiated mice (Figure S5B). Over 90% of all perilipin^{+} bone marrow adipocytes from these mice were Tomato^{+} (Figures S5B and S5D). Thus, *Lepr*$^{+}$ BMSCs generate most of the adipocytes formed in adult bone marrow.

Adult *Lepr*$^{+}$ BMSCs, but not perinatal chondrocytes, contribute to fracture healing

We investigated the contribution of perinatal chondrocytes and adult *Lepr*$^{+}$ BMSCs to bone regeneration. Safranin O staining revealed cartilage formation at the callus of the fractured femur (Figure 3A). Consistent with literature (Zhou et al., 2014b), administering tamoxifen to *Acan*^{creER}*; R26*^{tdTomato}*; Col1a1-GFP* mice during the facture healing process labeled cartilage and osteoblasts in the callus (Figure 3B). In contrast, few *Col1a1*-GFP^{+} osteoblasts were Tomato^{+} at the callus from *Acan*^{creER}*; R26*^{tdTomato}*; Col1a1-GFP* mice that had been treated with tamoxifen at P1–P3 (Figure 3C). 8 weeks after bone fracture, when the femur had largely healed (Figure 3A), almost no regenerated osteoblasts expressed Tomato in these mice (Figure 3D). Thus, perinatal chondrocytes do not generate progenitors for fracture healing.

We then performed fractures on 4-month-old *Lepr-creER; R26*^{tdTomato}*; Col1a1-GFP* mice that had been tamoxifen treated at 2 months of age. 2 weeks after fracture, Tomato expression was detected in a subset of *Col1a1*-GFP^{+} osteoblasts (Figure 3E) and aggrecan^{+} chondrocytes (Figure S5E). 8 weeks after bone fracture, some regenerated osteoblasts expressed Tomato in *Lepr-creER; R26*^{tdTomato}*; Col1a1-GFP* mice (Figure 3F). A few perivascular stromal cells were detected in the periosteum of the metaphysis from *Lepr-creER; R26*^{tdTomato}*; Col1a1-GFP* mice pulsed at 2 months of age, but they were not detected at the diaphysis where the fracture occurred (Figures S5F and S5G). Adult *Lepr*$^{+}$ BMSCs contribute to osteoblast regeneration upon injury.

Osteoblast-forming *Lepr*$^{+}$ cells derive from *Col2*$^{+}$ cells

Our data above suggested chondrocytes and *Lepr*$^{+}$ BMSCs as developmental and adult skeletal progenitors, respectively. To investigate the potential relationship between them, we used *Col2*-Cre (Hao et al., 2002) and *Lepr*-DreER, two different recombinases, to simultaneously trace chondrocytes and *Lepr*$^{+}$ BMSCs. Dre recombinase excises DNA regions flanked by rox recombination sites (Anastassiadis et al., 2009), activating Tomato expression when crossed with *Rosa26*$^{CAG\text{-}rox\text{-}STOP\text{-}rox\text{-}tdTomato}$ (*R26*$^{RSR\text{-}tdTomato}$) mice. *Lepr*-DreER did not show leaky recombination without tamoxifen treatment (Figure S6A). It recombined efficiently in LepR^{+} BMSCs but not in *Col1a1*-GFP^{+} osteoblasts, perilipin^{+} adipocytes, or aggrecan^{+} chondrocytes (Figures S6B–S6E). 3 weeks after tamoxifen treatment, robust labeling of *Col1a1*-GFP^{+} osteoblasts by Tomato was detected at diaphyseal bones (Figure S6F). In *Col2-cre; R26*^{tdTomato}*; Col1a1-GFP* mice, *Col2*-Cre marked cells included chondrocytes, periosteal cells, BMSCs, and osteoblasts (Figures S7A and S7B), consistent with previous reports (Ono et al., 2014; Szabova et al., 2009).

In *Col2-cre; Lepr*^{dreER}*; R26*$^{LSL\text{-}ZsGreen}$*; R26*$^{RSR\text{-}tdTomato}$ mice, *Lepr*-derived cells and *Col2*-derived cells were labeled by Tomato and ZsGreen, respectively (Figure 4A). Osteoblasts were marked by anti-Osx staining (Figures 4B and S5H–S5K). Mice were treated with tamoxifen 4 and 7 weeks after birth and analyzed at 10 weeks. Confocal imaging and flow cytometry analysis revealed significant overlap of most Tomato^{+} (*Lepr*-derived) and ZsGreen^{+} (*Col2*-derived) BMSCs (Figures 4B and 4C). Moreover, Tomato (*Lepr* derived) and ZsGreen (*Col2* derived) also displayed extensive overlap in Osx^{+} osteoblasts, especially at the diaphysis (Figure 4B). Similar results were obtained when *Acan*$^{+}$ progenitors and *Lepr*$^{+}$ BMSCs were traced simultaneously by *Acan*-Dre and *Lepr*-CreER, respectively (Figures S6G–S6I). Thus, *Col2*$^{+}$ progenitors, *Lepr*$^{+}$ BMSCs, and their osteolineages are genetically related.

The simultaneous tracing experiments could not tell which population is upstream of the other. To address this issue, we developed a mutually exclusive tracing system using the *R26*$^{CAG\text{-}loxp\text{-}rox\text{-}STOP\text{-}loxp\text{-}ZsGreen\text{-}rox\text{-}tdTomato}$ interleaved reporter (IR) (He et al., 2017). In *Col2*^{dre}*; Lepr*^{cre}*; IR* mice, *Lepr*-Cre- and *Col2*-Dre-mediated recombination was mutually exclusive in the same cell and its progeny. Whichever appeared first would prevent recombination by the other. This allowed us to determine which one appears first (Figure 4D). As expected, we never detected ZsGreen^{+}Tomato^{+} cells in *Col2*^{dre}*; Lepr*^{cre}*; IR* mice (Figures 4G and 4J).

Figure 4. Hierarchical organization among chondrocytes, *Lepr*$^{+}$ BMSCs, and their osteolineages

(A) Schematic showing the strategy for simultaneous tracing of chondrocytes and *Lepr*$^{+}$ BMSCs.

(B) Confocal imaging of femur sections from 10-week-old *Col2-cre; Lepr*^{dreER}*; R26*$^{LSL\text{-}ZsGreen}$*; R26*$^{RSR\text{-}tdTomato}$ mice that had been tamoxifen treated at 4 and 7 weeks of age. *Col2*- and *Lepr*-derived cells were marked by ZsGreen and Tomato, respectively. Osteoblasts were marked by anti-Osx staining. n = 3 mice from 3 independent experiments.

(C) Flow cytometry analysis of enzymatically dissociated bone marrow cells from 10-week-old *Col2-cre; Lepr*^{dreER}*; R26*$^{LSL\text{-}ZsGreen}$*; R26*$^{RSR\text{-}tdTomato}$ mice that had been tamoxifen-treated at 4 and 7 weeks of age. Bone marrow cells from *Col2-cre; R26*$^{LSL\text{-}ZsGreen}$ and *Lepr*^{dreER}*; R26*$^{RSR\text{-}tdTomato}$ mice were set as negative controls (gray peaks). n = 3 mice from 3 independent experiments.

(D) Schematic showing the strategy for mutually exclusive tracing of chondrocytes and *Lepr*$^{+}$ BMSCs.

(E–G) Flow cytometry analysis of whole bone marrow cells from 5-month-old *Col2*^{dre}*; IR* (E), *Lepr*^{cre}*; IR* (F) and *Col2*^{dre}*; Lepr*^{cre}*; IR* mice (G). n = 3 mice per genotype from 3 independent experiments.

(H–J) Confocal imaging of femur sections from 5-month-old *Col2*^{dre}*; IR* (H), *Lepr*^{cre}*; IR* (I) and *Col2*^{dre}*; Lepr*^{cre}*; IR* mice (J). Osteoblasts were marked by anti-Osx staining. n = 3 mice per genotype from 3 independent experiments.

See also Figure S6.

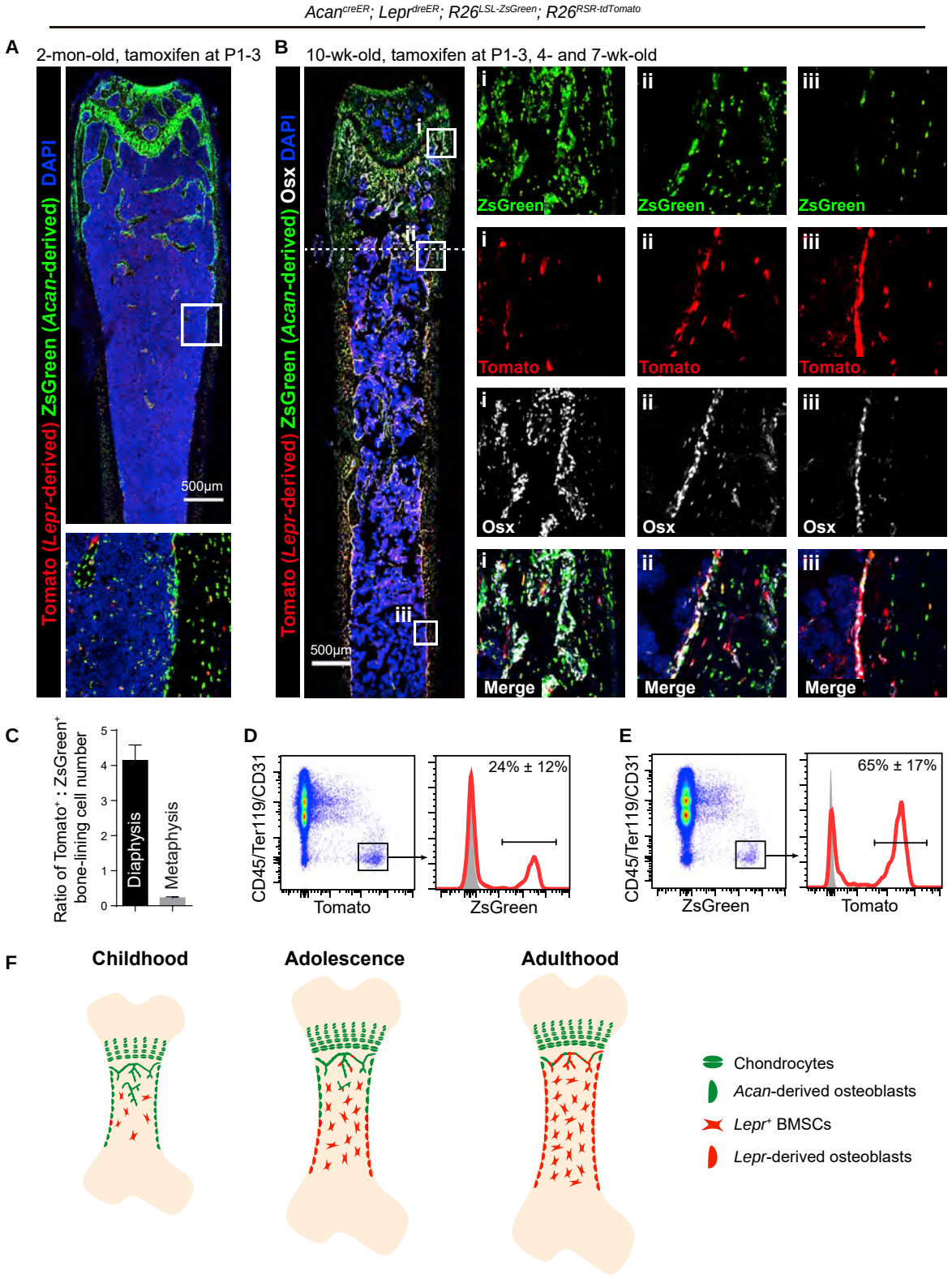

Figure 5. Chondrocytes and *Lepr*$^+$ BMSCs generate spatially separated subsets of osteoblasts during adolescence

(A) Confocal imaging of femur sections from 2-month-old *Acan*^{creER}; *Lepr*^{dreER}; *R26*$^{LSL\text{-}ZsGreen}$; *R26*$^{RSR\text{-}tdTomato}$ mice that had been tamoxifen-treated at P1–P3. n = 3 mice from 3 independent experiments.

(legend continued on next page)

Flow cytometry analysis showed that the frequencies of Tomato$^+$ cells in the bone marrow of 5-month-old *Col2^{dre}; IR* and *Col2^{dre}; Lepr^{cre}; IR* mice were comparable (Figures 4E and 4G). In contrast, the frequency of ZsGreen$^+$ cells in the bone marrow of *Col2^{dre}; Lepr^{cre}; IR* mice was only about 11% of that in *Lepr^{cre}; IR* mice (Figures 4F and 4G), suggesting that *Col2*-Dre-mediated recombination prevents *Lepr*-Cre-mediated recombination in most BMSCs. Consistent with this, femur sections of 5-month-old *Col2^{dre}; Lepr^{cre}; IR* mice largely resembled those of *Col2^{dre}; IR* mice, with few ZsGreen$^+$ BMSCs (Figures 4H–4J). Most Osx$^+$ osteoblasts were ZsGreen$^-$Tomato$^+$ (Figure 4J), suggesting that most *Lepr*-derived osteoblasts originate from *Col2*$^+$ cells. Thus, the *Col2* lineage is upstream of *Lepr*-derived BMSCs and osteoblasts.

Perinatal chondrocytes and *Lepr*$^+$ BMSCs form spatially separated subsets of osteoblasts during adolescence

To investigate the relationship between perinatal chondrocytes and *Lepr*$^+$ BMSCs, we generated *Acan^{creER}; Lepr^{dreER}; R26$^{LSL\text{-}ZsGreen}$; R26$^{RSR\text{-}tdTomato}$* mice. Femur sections from 2-month-old mice that had been tamoxifen treated at P1–P3 showed extensive labeling of BMSCs and bone-lining osteoblasts by ZsGreen but few by Tomato (Figure 5A), consistent with our finding that perinatal chondrocytes, but not *Lepr*$^+$ BMSCs, make the major contribution to osteoblast formation during childhood.

We next treated *Acan^{creER}; Lepr^{dreER}; R26$^{LSL\text{-}ZsGreen}$; R26$^{RSR\text{-}tdTomato}$* mice with tamoxifen 1 day, 4 weeks, and 7 weeks after birth. At 10 weeks of age, we observed a clear gradient formed by ZsGreen and Tomato fluorescence along the endosteum (Figure 5B). Osx$^+$ osteoblasts in the metaphysis were mostly ZsGreen$^+$Tomato$^-$ (*Acan* derived), whereas those in the diaphysis were mostly ZsGreen$^-$Tomato$^+$ (*Lepr* derived; Figures 5B and 5C), suggesting that perinatal chondrocytes and *Lepr*$^+$ BMSCs generate spatially separated subsets of osteoblasts in 10-week-old mice.

By flow cytometry, only a small subset of Tomato$^+$ (*Lepr*-derived) BMSCs were ZsGreen$^+$ (*Acan* derived) in *Acan^{creER}; Lepr^{dreER}; R26$^{LSL\text{-}ZsGreen}$; R26$^{RSR\text{-}tdTomato}$* mice (Figure 5D), although most of the ZsGreen$^+$ (*Acan* derived) BMSCs were Tomato$^+$ (*Lepr* derived; Figure 5E). Consistent with Figures 1H–1J, these data suggested that perinatal chondrocytes give rise to a small subset of *Lepr*$^+$ BMSCs.

Runx2 is required by perinatal chondrocytes for bone growth

Next we investigated the physiological importance of perinatal chondrocytes and *Lepr*$^+$ BMSCs in bone development and maintenance. We conditionally deleted *Runx2*, a master regulator of osteogenic differentiation (Komori et al., 1997; Otto et al., 1997), from these two populations. Two-month-old *Acan^{creER}; Runx2$^{fl/fl}$* mice that had been tamoxifen treated at P1–P3 had smaller body sizes than control mice (Figure 6A). Consistent with this, these mice had significantly shorter tails and femora compared with control mice (Figures 6A, 6B, and 6E). Micro-computed tomography (micro-CT) analysis showed that *Acan^{creER}; Runx2$^{fl/fl}$* mice had significantly reduced trabecular bone volume, trabecular number, trabecular thickness, and cortical area and significantly increased trabecular spacing compared with control mice (Figures 6C, 6D, and 6F–6L). These data suggest that deletion of *Runx2* from perinatal chondrocytes impairs bone growth, especially bone lengthening, during development.

In contrast, 4-month-old *Acan^{creER}; Runx2$^{fl/fl}$* mice that had been tamoxifen treated at 2 months of age showed normal bone parameters (Figures S7F–S7M), suggesting that adult chondrocytes are dispensable for bone formation.

Runx2 is required by *Lepr*$^+$ BMSCs for bone maintenance in adult mice

We used a non-inducible *Lepr*-Cre allele to delete *Runx2* (DeFalco et al., 2001). Two-month-old *Lepr^{cre}; Runx2$^{fl/fl}$* mice showed normal body size, normal femur length, and normal trabecular and cortical bone parameters (Figures 6M–6X), consistent with the limited contribution of *Lepr*$^+$ cells to osteoblasts during development. Four-month-old *Lepr^{cre}; Runx2$^{fl/fl}$* mice also had normal body size, normal femur length, and normal trabecular bone parameters but reduced cortical area and thickness (Figures 6Y–6AJ). Seven-month-old *Lepr^{cre}; Runx2$^{fl/fl}$* mice had more severe defects in bone formation because the defects appeared in trabecular and cortical parameters (Figures S7O–S7W). Reduced bone thickness was also observed in 4-month-old *Lepr-creER; Runx2$^{fl/fl}$* mice that were treated with tamoxifen at 2 months of age (Figures S7X–S7AF). These data suggested that conditional deletion of *Runx2* from *Lepr*$^+$ BMSCs impairs bone thickening in adult mice.

Running differentially regulates osteoblast formation by perinatal and adult skeletal progenitors

Finally we investigated how perinatal and adult skeletal progenitors respond to physiological stimuli, such as running. One-month-old *Acan^{creER}; R26^{tdTomato}; Col1a1-GFP* mice that had been tamoxifen treated at P1–P3 were subjected to forced running for 2 h once every day at a speed of 14 m/min (Figure 7A). Two months after running, the *Col1a1*-GFP$^+$ osteoblast pool contained significantly more Tomato$^+$ cells than controls by flow cytometry (Figures 7B–7D). Consistent with this, we observed more Tomato$^+$ osteoblasts in the diaphysis of *Acan^{creER}; R26^{tdTomato}; Col1a1-GFP* mice after running compared with controls (Figures 7E and 7F). These data suggest

(B and C) Confocal imaging of femur sections from 10-week-old *Acan^{creER}; Lepr^{dreER}; R26$^{LSL\text{-}ZsGreen}$; R26$^{RSR\text{-}tdTomato}$* mice that had been tamoxifen treated at P1–P3 and 4 and 7 weeks after birth. The white dashed line artificially separated the metaphysis from the diaphysis (B). *Acan*- and *Lepr*-derived cells were marked by ZsGreen and Tomato, respectively. Osteoblasts were marked by anti-Osx staining. The ratios of Tomato$^+$:ZsGreen$^+$ osteoblast numbers were quantified (C). n = 3 mice from 3 independent experiments.

(D and E) Flow cytometry analysis of enzymatically dissociated bone marrow cells from 10-week-old *Acan-creER; Lepr^{dreER}; R26$^{LSL\text{-}ZsGreen}$; R26$^{RSR\text{-}tdTomato}$* mice that had been tamoxifen treated at P1–P3, and 4 and 7 weeks after birth. n = 3 mice from 3 independent experiments.

(F) Schematic depicting the progenitor transition during postnatal bone growth. The contributions of perinatal chondrocytes and *Lepr*$^+$ BMSCs to osteoblast formation are separated temporally and spatially.

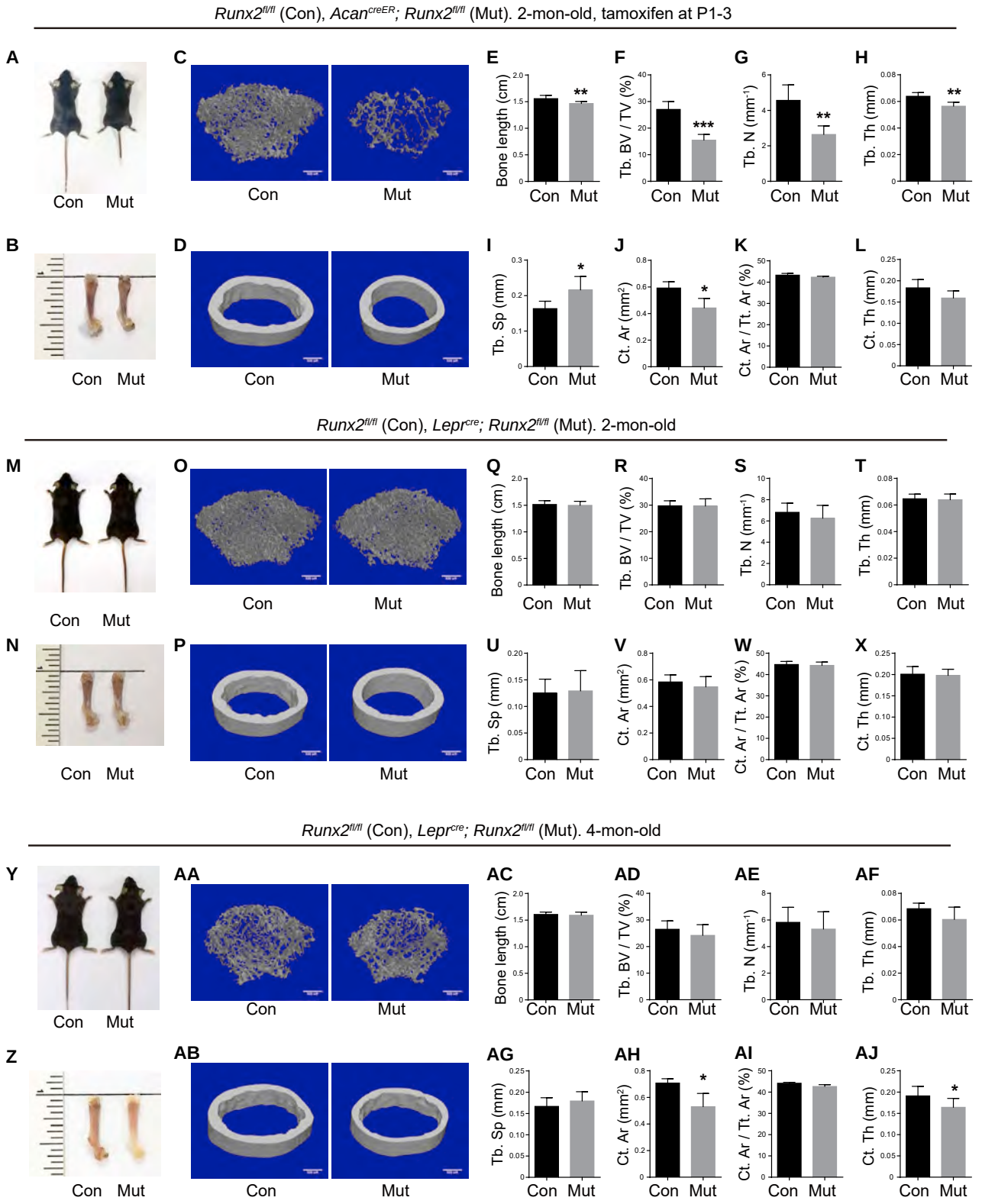

Figure 6. Deletion of *Runx2* from perinatal chondrocytes and from adult *Lepr*$^{+}$ BMSCs impairs bone lengthening and thickening, respectively

Different sexes were examined in different experiments so that most data reflected male and female mice. Two-tailed Student's t tests were used to assess the statistical significance of differences between sex-matched littermates (*$p < 0.05$, **$p < 0.01$, ***$p < 0.001$).

(legend continued on next page)

that running augments osteoblast formation by chondrocytes in juvenile mice.

In contrast, when 3-month-old *Lepr-creER; R26*^{tdTomato}*; Col1a1-GFP* mice that had been tamoxifen treated at 2 months of age were subjected to running for 2 months (Figure 7G), we did not detect significant changes in the frequency of Tomato$^+$ osteoblasts of these mice by flow cytometry (Figures 7H–7J) or by confocal imaging (Figures 7K and 7L). These data suggest that running does not affect osteoblast formation by adult *Lepr*$^+$ BMSCs.

DISCUSSION

Our work has established that postnatal osteoblast production by chondrocytes and BMSCs is separated temporally and spatially. This skeletal progenitor transition occurs during adolescence, which explains, from a stem cell perspective, why mouse endochondral bones transition from rapid longitudinal growth to slower appositional remodeling after adolescence. By inducible lineage tracing, we provided direct evidence that adult *Lepr*$^+$ BMSCs are self-renewable. Interestingly, a recent study identified a subpopulation of *Lepr*$^+$ BMSCs that expressed *osteolectin* (Shen et al., 2021). The *Lepr*$^+$*osteolectin*$^+$ cells were short-lived osteogenic progenitors. Combined with our data, it revealed a hierarchy in adult skeletal stem cells: the self-renewable skeletal stem cells enriched in *Lepr*$^+$*osteolectin*$^-$ BMSCs give rise to the short-lived *Lepr*$^+$*osteolectin*$^+$ osteogenic progenitors. These cells actively form osteoblasts and are replaced continuously by new *Lepr*$^+$ *osteolectin*$^+$ cells during aging.

Col2-Cre-marked cells gave rise to ~70%, not all, of *Lepr*$^+$ BMSCs (Figure 4C). One possibility is that *Col2*-Cre did not recombine in all chondrocytes. If *Col2*-Cre worked as expected, then this would raise the possibility that the remaining 30% of unlabeled *Lepr*$^+$ BMSCs are formed by cells other than *Col2*$^+$ cells. One candidate is perichondral Osx$^+$ cells (Maes et al., 2010; Matsushita et al., 2020; Mizoguchi et al., 2014). Some may be generated through endothelial-to-mesenchymal transition (Kenswil et al., 2021). Future studies need to determine the other cells of origin of adult skeletal progenitors and osteoblasts.

LIMITATIONS OF THE STUDY

Unlike *Acan*-CreER, *Col2*-Cre also marked periosteal cells (compare Figures S1C and S7A; Szabova et al., 2009). *Acan*-Dre might have the same pattern. It is currently difficult to distinguish the fates of chondrocytes and periosteal cells marked by *Col2*-Cre. Nevertheless, we found that *Col10*-Cre-marked cells, which excluded periosteal cells (Figure S7C), gave rise to ~58% of all *Lepr*$^+$ BMSCs (Figures S7D and S7E), whereas *Col2*-Cre-marked cells give rise to ~70% (Figure 4C). Thus, there were ~12% of *Lepr*$^+$ BMSCs that might derive from *Col2*$^+$*Col10*$^-$ periosteal cells. On one hand, it suggested that we overestimated the contribution of fetal chondrocytes to adult skeletal progenitors; on the other hand, it implied that some adult skeletal progenitors derive from the periosteum. Because the periosteal collar is made by an intramembranous process, this suggests that intramembranous and endochondral bone formation are actually one spectrum. Moreover, only a minor fraction of chondrocytes and osteoblasts at the callus derived from *Lepr*$^+$ BMSCs during fracture healing (Figures S5E and 3E), supporting the idea that periosteal cells are also involved in fracture healing (Debnath et al., 2018; Ortinau et al., 2019). It will be particularly interesting and important to generate tools to distinguish the fates of progenitors from the growth plate, bone marrow, and periosteum and to dissect their division of labor during bone growth, remodeling, and regeneration.

STAR★METHODS

Detailed methods are provided in the online version of this paper and include the following:

- KEY RESOURCES TABLE
- RESOURCE AVAILABILITY
  - Lead contact
  - Materials availability
  - Data and code availability
- EXPERIMENTAL MODEL AND SUBJECT DETAILS
  - Animal models
- METHOD DETAILS

(A and B) Representative images of *Runx2*$^{fl/fl}$ (control, Con) and *Acan*^{creER}*; Runx2*$^{fl/fl}$ (mutant, Mut) mice that had been tamoxifen treated at P1–P3 (A) and their femora (B). n = 5 mice from 5 independent experiments.

(C and D) Representative micro-CT images showing trabecular (C) and cortical bones (D) from 2-month-old *Runx2*$^{fl/fl}$ (Con) and *Acan*^{creER}*; Runx2*$^{fl/fl}$ (Mut) mice that had been tamoxifen treated at P1–P3. n = 5 mice from 5 independent experiments.

(E–L) Femur length (E), trabecular bone volume/total bone volume (Tb. BV/TV; F), trabecular number (Tb. N; G), thickness (Tb. Th; H), spacing (Tb. Sp; I), cortical area (Ct. Ar; J), cortical area/total area (Ct. Ar/Tt. Ar; K), and thickness (Ct. Th; L) of femora from 2-month-old *Runx2*$^{fl/fl}$ (Con) and *Acan*^{creER}*; Runx2*$^{fl/fl}$ (Mut) mice. All data represent mean ± SD of 5 mice per genotype from 5 independent experiments.

(M and N) Representative images of 2-month-old *Runx2*$^{fl/fl}$ (Con) and *Lepr*^{cre}*; Runx2*$^{fl/fl}$ (Mut) mice (M) and their femora (N). n = 5 mice from 5 independent experiments.

(O and P) Representative micro-CT images showing trabecular (O) and cortical bones (P) from 2-month-old *Runx2*$^{fl/fl}$ (Con) and *Lepr*^{cre}*; Runx2*$^{fl/fl}$ (Mut) mice. n = 5 mice from 5 independent experiments.

(Q–X) Femur length (Q), Tb. BV/TV (R), Tb. N (S), Tb. Th (T), Tb. Sp (U), Ct. Ar (V), Ct. Ar/Tt. Ar (W), and Ct. Th (X) of femora from 2-month-old *Runx2*$^{fl/fl}$ (Con) and *Lepr*^{cre}*; Runx2*$^{fl/fl}$ (Mut) mice. All data represent mean ± SD of 5 mice per genotype from 5 independent experiments.

(Y and Z) Representative images of 4-month-old *Runx2*$^{fl/fl}$ (Con) and *Lepr*^{cre}*; Runx2*$^{fl/fl}$ (Mut) mice (Y) and their femora (Z). n = 5 mice from 5 independent experiments.

(AA and AB) Representative micro-CT images showing trabecular (AA) and cortical bones (AB) from 4-month-old *Runx2*$^{fl/fl}$ (Con) and *Lepr*^{cre}*; Runx2*$^{fl/fl}$ (Mut) mice. n = 5 mice from 5 independent experiments.

(AC–AJ) Femur length (AC), Tb. BV/TV (AD), Tb. N (AE), Tb. Th (AF), Tb. Sp (AG), Ct. Ar (AH), Ct. Ar/Tt. Ar (AI), and Ct. Th (AJ) of femora from 4-month-old *Runx2*$^{fl/fl}$ (Con) and *Lepr*^{cre}*; Runx2*$^{fl/fl}$ (Mut) mice. All data represent mean ± SD of 5 mice per genotype from 5 independent experiments.

See also Figure S7.

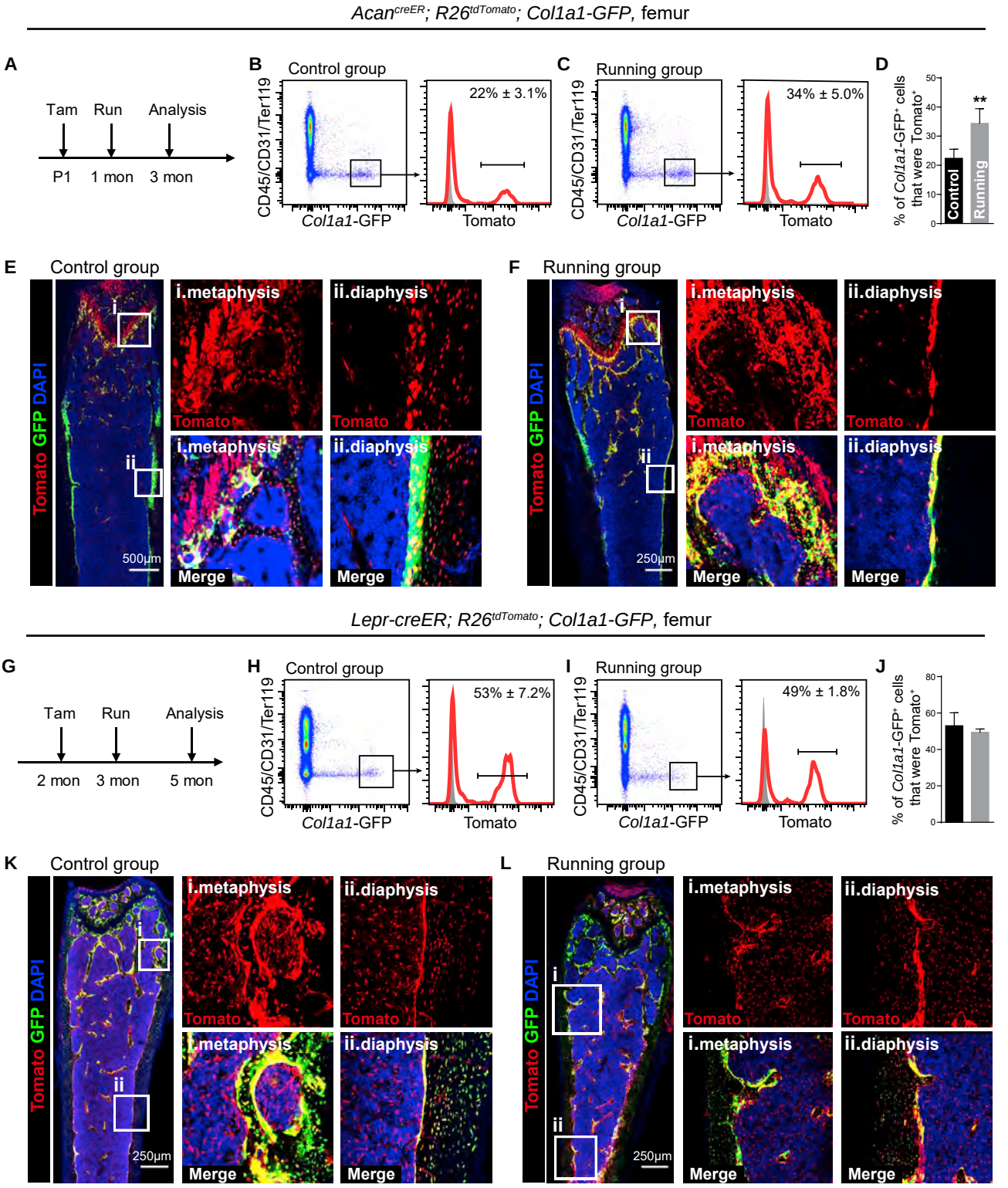

Figure 7. Forced running significantly increases osteoblast formation by perinatal chondrocytes but not by adult *Lepr*$^{+}$ BMSCs

(A) Schematic showing the experimental timeline for *Acan*^{creER}; *R26*^{tdTomato}; *Col1a1-GFP* mice.

(B–D) Flow cytometry analyses of femora from *Acan*^{creER}; *R26*^{tdTomato}; *Col1a1-GFP* mice with (C) or without running (B) and quantification of percentages of *Col1a1*-GFP^{+} osteoblasts that were Tomato^{+} in the femora from the control and the running group (D). Data represent mean ± SD of 5 mice per condition from 5 independent experiments. Two-tailed Student's t tests were used to assess the statistical significance of differences (**$p < 0.01$).

(legend continued on next page)

- Tamoxifen treatment
- Flow cytometry of whole bone marrow cells
- Flow cytometry of femur shafts
- Immunofluorescence and confocal imaging
- Safranin O Staining
- Running experiments
- Micro-CT analysis
- CFU-F forming efficiency assay
- Bone fracture
- Lethal irradiation and bone marrow transplantation

● QUANTIFICATION AND STATISTICAL ANALYSIS

SUPPLEMENTAL INFORMATION

Supplemental information can be found online at https://doi.org/10.1016/j.stem.2021.08.010.

ACKNOWLEDGMENTS

This work was supported by the National Key Program on Stem Cell and Translational Research (2018YFA0107200 and 2017YFA0106400), the Strategic Priority Research Program on Stem Cell and Translational Research (XDA16020202), the National Natural Science Foundation of China (31771637 and 81730006), and a pilot research grant from State Key Laboratory of Experimental Hematology (ZK20-08). We thank Dr. Sean J. Morrison at UT Southwestern Medical Center for suggestions and careful editing of the manuscript, Dr. Yugang Gao at Binzhou Medical University for providing the *Runx2*$^{fl/+}$ mice, and Dr. Xiao Yang at the Beijing Institute of Lifeomics for providing the *Col2-cre* mice.

AUTHOR CONTRIBUTIONS

H.S.S. and B.O.Z. initiated the project. H.S.S. performed most of the imaging and flow cytometry experiments. Y.L.L. performed the running exercise experiments and was involved in micro-CT analysis. X.T.T. and X.S.Z. participated in some of the confocal imaging experiments. B.Z. provided the *R26*$^{RSR\text{-}tdTomato}$ and IR mice. W.Z. maintained the *Acan*^{creER} mice. B.O.Z. and H.S.S. wrote the manuscript and interpreted the data.

DECLARATION OF INTERESTS

The authors declare no competing interests.

Received: August 5, 2020
Revised: February 23, 2021
Accepted: August 12, 2021
Published: September 8, 2021

REFERENCES

Anastassiadis, K., Fu, J., Patsch, C., Hu, S., Weidlich, S., Duerschke, K., Buchholz, F., Edenhofer, F., and Stewart, A.F. (2009). Dre recombinase, like Cre, is a highly efficient site-specific recombinase in E. coli, mammalian cells and mice. Dis. Model. Mech. *2*, 508–515.

Baryawno, N., Przybylski, D., Kowalczyk, M.S., Kfoury, Y., Severe, N., Gustafsson, K., Kokkaliaris, K.D., Mercier, F., Tabaka, M., Hofree, M., et al. (2019). A Cellular Taxonomy of the Bone Marrow Stroma in Homeostasis and Leukemia. Cell *177*, 1915–1932.e16.

Bouxsein, M.L., Boyd, S.K., Christiansen, B.A., Guldberg, R.E., Jepsen, K.J., and Muller, R. (2010). Guidelines for assessment of bone microstructure in rodents using micro-computed tomography. J. Bone Miner. Res. *25*, 1468–1486.

Chu, Q., Gao, Y., Gao, X., Dong, Z., Song, W., Xu, Z., Xiang, L., Wang, Y., Zhang, L., Li, M., and Gao, Y. (2018). Ablation of Runx2 in Ameloblasts Suppresses Enamel Maturation in Tooth Development. Sci. Rep. *8*, 9594.

Debnath, S., Yallowitz, A.R., McCormick, J., Lalani, S., Zhang, T., Xu, R., Li, N., Liu, Y., Yang, Y.S., Eiseman, M., et al. (2018). Discovery of a periosteal stem cell mediating intramembranous bone formation. Nature *562*, 133–139.

DeFalco, J., Tomishima, M., Liu, H., Zhao, C., Cai, X., Marth, J.D., Enquist, L., and Friedman, J.M. (2001). Virus-assisted mapping of neural inputs to a feeding center in the hypothalamus. Science *291*, 2608–2613.

Duchamp de Lageneste, O., Julien, A., Abou-Khalil, R., Frangi, G., Carvalho, C., Cagnard, N., Cordier, C., Conway, S.J., and Colnot, C. (2018). Periosteum contains skeletal stem cells with high bone regenerative potential controlled by Periostin. Nat. Commun. *9*, 773.

Hao, Z.M., Yang, X., Cheng, X., Zhou, J., and Huang, C.F. (2002). [Generation and characterization of chondrocyte specific Cre transgenic mice]. Yi Chuan Xue Bao *29*, 424–429.

He, L., Li, Y., Li, Y., Pu, W., Huang, X., Tian, X., Wang, Y., Zhang, H., Liu, Q., Zhang, L., et al. (2017). Enhancing the precision of genetic lineage tracing using dual recombinases. Nat. Med. *23*, 1488–1498.

Henry, S.P., Jang, C.W., Deng, J.M., Zhang, Z., Behringer, R.R., and de Crombrugghe, B. (2009). Generation of aggrecan-CreERT2 knockin mice for inducible Cre activity in adult cartilage. Genesis *47*, 805–814.

Kalajzic, Z., Liu, P., Kalajzic, I., Du, Z., Braut, A., Mina, M., Canalis, E., and Rowe, D.W. (2002). Directing the expression of a green fluorescent protein transgene in differentiated osteoblasts: comparison between rat type I collagen and rat osteocalcin promoters. Bone *31*, 654–660.

Kenswil, K.J.G., Pisterzi, P., Sánchez-Duffhues, G., van Dijk, C., Lolli, A., Knuth, C., Vanchin, B., Jaramillo, A.C., Hoogenboezem, R.M., Sanders, M.A., et al. (2021). Endothelium-derived stromal cells contribute to hematopoietic bone marrow niche formation. Cell Stem Cell *28*, 653–670.e11.

Komori, T., Yagi, H., Nomura, S., Yamaguchi, A., Sasaki, K., Deguchi, K., Shimizu, Y., Bronson, R.T., Gao, Y.H., Inada, M., et al. (1997). Targeted disruption of Cbfa1 results in a complete lack of bone formation owing to maturational arrest of osteoblasts. Cell *89*, 755–764.

Madisen, L., Zwingman, T.A., Sunkin, S.M., Oh, S.W., Zariwala, H.A., Gu, H., Ng, L.L., Palmiter, R.D., Hawrylycz, M.J., Jones, A.R., et al. (2010). A robust and high-throughput Cre reporting and characterization system for the whole mouse brain. Nat. Neurosci. *13*, 133–140.

Madisen, L., Garner, A.R., Shimaoka, D., Chuong, A.S., Klapoetke, N.C., Li, L., van der Bourg, A., Niino, Y., Egolf, L., Monetti, C., et al. (2015). Transgenic mice for intersectional targeting of neural sensors and effectors with high specificity and performance. Neuron *85*, 942–958.

Maes, C., Kobayashi, T., Selig, M.K., Torrekens, S., Roth, S.I., Mackem, S., Carmeliet, G., and Kronenberg, H.M. (2010). Osteoblast precursors, but not mature osteoblasts, move into developing and fractured bones along with invading blood vessels. Dev. Cell *19*, 329–344.

Marędziak, M., Śmieszek, A., Chrząstek, K., Basinska, K., and Marycz, K. (2015). Physical Activity Increases the Total Number of Bone-Marrow-Derived Mesenchymal Stem Cells, Enhances Their Osteogenic Potential, and Inhibits Their Adipogenic Properties. Stem Cells Int. *2015*, 379093.

(E and F) Confocal imaging of femur sections from *Acan*^{creER}*; R26*^{tdTomato}*; Col1a1-GFP* mice with (F) or without running (E). n = 3 mice per condition from 3 independent experiments.
(G) Schematic showing the experimental timeline for *Lepr-creER; R26*^{tdTomato}*; Col1a1-GFP* mice.
(H–J) Flow cytometric analyses of femora from *Lepr-creER; R26*^{tdTomato}*; Col1a1-GFP* mice with (I) or without running (H). Quantification of percentages of *Col1a1*-GFP^{+} osteoblasts that were Tomato^{+} in the femora from the control and the running group (J). Data represent mean ± SD of 5 mice per condition from 5 independent experiments. Two-tailed Student's t tests were used to assess the statistical significance of differences.
(K and L) Confocal imaging of femur sections from *Lepr-creER; R26*^{tdTomato}*; Col1a1-GFP* mice with (L) or without running (K). n = 3 mice per condition from 3 independent experiments.

Matsushita, Y., Nagata, M., Welch, J.D., Wong, S.Y., Ono, W., and Noriaki Ono, N. (2020). Notch effector Hes1 marks an early perichondrial population of skeletal 1 progenitor cells at the onset of endochondral bone development. bioRxiv. https://doi.org/10.1101/2020.03.13.990853.

Méndez-Ferrer, S., Michurina, T.V., Ferraro, F., Mazloom, A.R., Macarthur, B.D., Lira, S.A., Scadden, D.T., Ma'ayan, A., Enikolopov, G.N., and Frenette, P.S. (2010). Mesenchymal and haematopoietic stem cells form a unique bone marrow niche. Nature *466*, 829–834.

Mizoguchi, T., Pinho, S., Ahmed, J., Kunisaki, Y., Hanoun, M., Mendelson, A., Ono, N., Kronenberg, H.M., and Frenette, P.S. (2014). Osterix marks distinct waves of primitive and definitive stromal progenitors during bone marrow development. Dev. Cell *29*, 340–349.

Mizuhashi, K., Ono, W., Matsushita, Y., Sakagami, N., Takahashi, A., Saunders, T.L., Nagasawa, T., Kronenberg, H.M., and Ono, N. (2018). Resting zone of the growth plate houses a unique class of skeletal stem cells. Nature *563*, 254–258.

Ono, N., Ono, W., Nagasawa, T., and Kronenberg, H.M. (2014). A subset of chondrogenic cells provides early mesenchymal progenitors in growing bones. Nat. Cell Biol. *16*, 1157–1167.

Ono, N., Balani, D.H., and Kronenberg, H.M. (2019). Stem and progenitor cells in skeletal development. Curr. Top. Dev. Biol. *133*, 1–24.

Ortinau, L.C., Wang, H., Lei, K., Deveza, L., Jeong, Y., Hara, Y., Grafe, I., Rosenfeld, S.B., Lee, D., Lee, B., et al. (2019). Identification of Functionally Distinct Mx1+αSMA+ Periosteal Skeletal Stem Cells. Cell Stem Cell *25*, 784–796.e5.

Otto, F., Thornell, A.P., Crompton, T., Denzel, A., Gilmour, K.C., Rosewell, I.R., Stamp, G.W., Beddington, R.S., Mundlos, S., Olsen, B.R., et al. (1997). Cbfa1, a candidate gene for cleidocranial dysplasia syndrome, is essential for osteoblast differentiation and bone development. Cell *89*, 765–771.

Park, D., Spencer, J.A., Koh, B.I., Kobayashi, T., Fujisaki, J., Clemens, T.L., Lin, C.P., Kronenberg, H.M., and Scadden, D.T. (2012). Endogenous bone marrow MSCs are dynamic, fate-restricted participants in bone maintenance and regeneration. Cell Stem Cell *10*, 259–272.

Pineault, K.M., Song, J.Y., Kozloff, K.M., Lucas, D., and Wellik, D.M. (2019). Hox11 expressing regional skeletal stem cells are progenitors for osteoblasts, chondrocytes and adipocytes throughout life. Nat. Commun. *10*, 3168.

Rux, D.R., Song, J.Y., Swinehart, I.T., Pineault, K.M., Schlientz, A.J., Trulik, K.G., Goldstein, S.A., Kozloff, K.M., Lucas, D., and Wellik, D.M. (2016). Regionally Restricted Hox Function in Adult Bone Marrow Multipotent Mesenchymal Stem/Stromal Cells. Dev. Cell *39*, 653–666.

Seike, M., Omatsu, Y., Watanabe, H., Kondoh, G., and Nagasawa, T. (2018). Stem cell niche-specific Ebf3 maintains the bone marrow cavity. Genes Dev. *32*, 359–372.

Shen, B., Tasdogan, A., Ubellacker, J.M., Zhang, J., Nosyreva, E.D., Du, L., Murphy, M.M., Hu, S., Yi, Y., Kara, N., et al. (2021). A mechanosensitive peri-arteriolar niche for osteogenesis and lymphopoiesis. Nature *591*, 438–444.

Szabova, L., Yamada, S.S., Wimer, H., Chrysovergis, K., Ingvarsen, S., Behrendt, N., Engelholm, L.H., and Holmbeck, K. (2009). MT1-MMP and type II collagen specify skeletal stem cells and their bone and cartilage progeny. J. Bone Miner. Res. *24*, 1905–1916.

Tikhonova, A.N., Dolgalev, I., Hu, H., Sivaraj, K.K., Hoxha, E., Cuesta-Domínguez, Á., Pinho, S., Akhmetzyanova, I., Gao, J., Witkowski, M., et al. (2019). The bone marrow microenvironment at single-cell resolution. Nature *569*, 222–228.

Worthley, D.L., Churchill, M., Compton, J.T., Tailor, Y., Rao, M., Si, Y., Levin, D., Schwartz, M.G., Uygur, A., Hayakawa, Y., et al. (2015). Gremlin 1 identifies a skeletal stem cell with bone, cartilage, and reticular stromal potential. Cell *160*, 269–284.

Yang, G., Zhu, L., Hou, N., Lan, Y., Wu, X.M., Zhou, B., Teng, Y., and Yang, X. (2014a). Osteogenic fate of hypertrophic chondrocytes. Cell Res. *24*, 1266–1269.

Yang, L., Tsang, K.Y., Tang, H.C., Chan, D., and Cheah, K.S. (2014b). Hypertrophic chondrocytes can become osteoblasts and osteocytes in endochondral bone formation. Proc. Natl. Acad. Sci. USA *111*, 12097–12102.

Zhou, B.O., Yue, R., Murphy, M.M., Peyer, J.G., and Morrison, S.J. (2014a). Leptin-receptor-expressing mesenchymal stromal cells represent the main source of bone formed by adult bone marrow. Cell Stem Cell *15*, 154–168.

Zhou, X., von der Mark, K., Henry, S., Norton, W., Adams, H., and de Crombrugghe, B. (2014b). Chondrocytes transdifferentiate into osteoblasts in endochondral bone during development, postnatal growth and fracture healing in mice. PLoS Genet. *10*, e1004820.

STAR★METHODS

KEY RESOURCES TABLE

REAGENT or RESOURCE	SOURCE	IDENTIFIER
Antibodies		
FITC anti-mouse CD45 Antibody	Biolegend	Cat#103108; RRID:AB_312973
FITC anti-mouse CD31 Antibody	Biolegend	Cat#102406; RRID:AB_312900
FITC anti-mouse TER-119/Erythroid Cells Antibody	Biolegend	Cat#116206; RRID:AB_313707
Biotin anti-mouse CD140a Antibody	Biolegend	Cat#135910; RRID:AB_2043974
Mouse Leptin R Biotinylated Antibody	R&D	Cat#BAF497; RRID:AB_2296953
APC anti-mouse CD45 Antibody	Biolegend	Cat#103112; RRID:AB_312977
APC anti-mouse CD31 Antibody	Biolegend	Cat#102410; RRID:AB_312905
APC anti-mouse TER-119/Erythroid Cells Antibody	Biolegend	Cat#116212; RRID:AB_313713
Mouse Endoglin/CD105 Antibody	R&D	Cat#AF1320; RRID:AB_2098896
Anti-Perilipin A/B antibody produced in rabbit	Sigma	Cat#P1873; RRID:AB_532267
Rabbit polyclonal anti-Aggrecan	Millipore	Cat#AB1031; RRID:AB_90460
Rabbit polyclonal anti-Collagen X	Abcam	Cat#ab58632; RRID:AB_879742
Rabbit polyclonal anti-Sox9	Millipore	Cat#AB5535; RRID:AB_2239761
Goat polyclonal anti-Sclerostin	R&D	Cat#AF1589-SP; RRID:AB_2195345
Goat polyclonal anti-Opn	R&D	Cat#AF808; RRID:AB_2194992
Rabbit polyclonal anti-Ocn	Abcam	Cat#ab93876; RRID:AB_10675660
Rabbit polyclonal anti-Col1	Abcam	Cat#ab292; RRID:AB_303415
Rabbit polyclonal anti-Sp7	Abcam	Cat#ab209484; RRID:AB_2892207
Anti rabbit Alexa Fluor 488	Invitrogen	Cat#A21206; RRID:AB_2535792
Anti rabbit Alexa Fluor 647	Invitrogen	Cat#A31573; RRID:AB_2536183
Anti goat Alexa Fluor 488	Invitrogen	Cat#A11055; RRID:AB_2534102
Anti goat Alexa Fluor 647	Invitrogen	Cat#A21447; RRID:AB_141844
APC Streptavidin	eBioscience	Cat#17-4317-82
Brilliant Violet 421 Streptavidin	Biolegend	Cat#405225
Chemicals, peptides, and recombinant proteins		
Tamoxifen	Sigma	Cat# T5648
4-Hydroxy-tamoxifen	Sigma	Cat# 579002
DAPI	Sigma	Cat# D9542
HBSS buffer	ThermoFisher	Cat# 14025134
Collagenase, Type 1	Worthington	Cat# LS004197
Collagenase, Type 4	Worthington	Cat# LS004189
DNase I from bovine pancreas	Sigma	Cat# 11284932001
OCT	ThermoFisher	Cat# NEG-50-6502
ProLong Gold Antifade	Invitrogen	Cat# P36930
Experimental models: Organisms/strains		
Mouse: *Col1a1*2.3-GFP*	The Jackson Laboratory	JAX:013134
Mouse: *R26*$^{CAG\text{-}loxp\text{-}STOP\text{-}loxp\text{-}tdTomato}$	The Jackson Laboratory	JAX:007909
Mouse: *R26*$^{CAG\text{-}rox\text{-}STOP\text{-}rox\text{-}loxp\text{-}STOP\text{-}loxp\text{-}tdTomato}$	The Jackson Laboratory	JAX:021876
Mouse: *R26*$^{CAG\text{-}loxp\text{-}STOP\text{-}loxp\text{-}Zsgreen}$	The Jackson Laboratory	JAX:007906
Mouse: *Acan*^{creER}	The Jackson Laboratory	JAX:019148
Mouse: *Lepr*^{cre}	The Jackson Laboratory	JAX:008320
Mouse: *ACTB-cre*	The Jackson Laboratory	JAX:019099
Mouse: *R26*$^{CAG\text{-}loxp\text{-}rox\text{-}STOP\text{-}loxp\text{-}ZsGreen\text{-}rox\text{-}tdTomato}$	Dr. Bin Zhou	He et al., 2017
Mouse: *Col2-cre*	Dr. Xiao Yang	Hao et al., 2002

(*Continued on next page*)

Continued

REAGENT or RESOURCE	SOURCE	IDENTIFIER
Mouse: *Runx2*$^{fl/+}$	Dr. Yugang Gao	Chu et al., 2018
Mouse: *Col10*^{cre}	This paper	Beijing Biocytogen Co., Ltd
Mouse: *Lepr-creER*	This paper	Cyagen Biosciences Inc.
Mouse: *Lepr*^{dreER}	This paper	Shanghai Biomodel Organism Co., Ltd
Mouse: *Col2*^{dre}	This paper	Shanghai Biomodel Organism Co., Ltd
Mouse: *Acan*^{dre}	This paper	Shanghai Biomodel Organism Co., Ltd
Software and algorithms		
Imagej	Fiji.sc	N/A
FlowJo	FLOWJO LLC	N/A
GraphPad Prism 7	GraphPad Software, inc	N/A

RESOURCE AVAILABILITY

Lead contact

Further information and requests for resources and reagents should be directed to and will be fulfilled by the lead contact, Bo O. Zhou (bo.zhou@sibcb.ac.cn).

Materials availability

New mouse lines generated in this study will be provided by the lead contact upon request.

Data and code availability

This study did not generate large datasets.

EXPERIMENTAL MODEL AND SUBJECT DETAILS

Animal models

All mice were maintained under C57BL/6 background in the Animal Facility at Shanghai Institute of Biochemistry and Cell Biology (SIBCB), Chinese Academy of Sciences. *R26*$^{RSR\text{-}tdTomato}$ mice were generated by crossing *Actb-cre* with *R26*$^{CAG\text{-}rox\text{-}Stop\text{-}rox\text{-}loxP\text{-}Stop\text{-}loxP\text{-}tdTomato}$ mice (Madisen et al., 2015) to excise the second loxP-flanked stop cassette. *Lepr-creER* transgenic mouse line was generated by injecting the BAC clone RP23-184F13, in which the *Lepr* gene locus was inserted with the *creER* sequence, into the fertilized eggs from C57BL/6 mice. *Lepr*^{dreER} knock-in mouse line was generated by knocking the *dreER* sequence into the endogenous *Lepr* gene locus. *Col2*^{dre} knock-in mouse line was generated by knocking the *dre* sequence into the endogenous *Col2* gene locus. Dre recombinase excises DNA regions flanked by rox recombination sites, together with Cre, allowing simultaneous tracing of two independent cell population. In the interleaved reporter (IR) mice, recombination by one recombinase should inherently remove one recombinase-recognition site of the other system to render its reporter inert to subsequent recombination (for example, recombination using Dre–rox should remove one loxP site and prevent subsequent Cre–loxP-mediated recombination). All mouse procedures were approved by the Institutional Animal Care and Use Committees of SIBCB.

METHOD DETAILS

Tamoxifen treatment

For perinatal induction of CreER activity, mice were intraperitoneally injected with 30 μg 4-OH tamoxifen at postnatal days 1 to 3. Otherwise, mice were intraperitoneally injected with 100 μL tamoxifen (10 mg/ml) for 5 days. For induction of DreER activity in juvenile mice, mice were intraperitoneally injected with 100 μL tamoxifen for 3 days at 4 and 7 weeks after birth, respectively.

Flow cytometry of whole bone marrow cells

Bone marrow was flushed from femur with 1 mL HBSS digestion buffer containing 5 mg Collagenase I, 5 mg Collagenase IV and 0.1 mg Dnase I and incubated in a shaking bath at 37°C for 30 minutes. Digested cells were centrifuged in 4°C centrifuge at 1500 rpm for 5 minutes. Supernatant was discarded, cells were suspended with 100 μL HBSS buffer and incubated for 30 minutes on ice with the following antibodies: CD45-FITC, Ter119-FITC. PDGFRα-biotin, LepR-biotin. Streptavidin-APC or Streptavidin-brilliant violet 421 were used as secondary antibodies. Flow cytometry was performed on Attune NxT flow cytometer (Thermo).

Flow cytometry of femur shafts

Marrow-depleted femurs were first cut to small pieces by scissors. Fragments were digested in 37°C shaking bath in 1 mL HBSS digestion buffer (same as above). 30 minutes later, HBSS was transferred into a new 5 mL FACS tube. 1 mL pre-warmed HBSS digestion buffer was added to fragments for another 30 minutes digestion. Digested cells were centrifuged in 4°C centrifuge at 1500 rpm for 5 minutes. Supernatant was discarded and cells were suspended with 100 μL HBSS buffer and incubated for 30 minutes on ice with the following antibodies: CD45-APC, CD31-APC, Ter119-APC. Flow cytometry was performed on Attune NxT flow cytometer (Thermo).

Immunofluorescence and confocal imaging

Femurs were fixed in 4% PFA overnight at 4°C and followed by 5-day decalcification in 20% EDTA. OCT-embedded femurs were sectioned using the CryoJane tape-transfer system (Leica Biosystems). Sections were blocked in PBS with 5% donkey serum and 0.1% triton for 1 hour and then stained overnight with primary antibodies. Primary antibodies used in this study were listed as above. Non-immune immunoglobulins of the same isotype as the primary antibodies were used as negative controls. Images were acquired by Leica TCS SP8 WLL or Leica TCS SP8 STED confocal microscope.

Safranin O Staining

Decalcified bones were dehydrated in ethanol step by step (75%, 85%, 95%, 100%). Subsequently, the specimens were embedded in paraffin and sectioned at 10 μm by Leica manual rotary microtome (Leica RM2235). Prepared paraffin sections went through dewaxing, hydration, and stained with safranin O and fast green. Finally, Slides were mounted with neutral mounting medium and images were acquired by BX51 (Olympus).

Running experiments

Forced running were performed according to literature (Marędziak et al., 2015). Mice were forced to run by putting them on the SA101 treadmill (SANS Biotechnology, China) for 2 hours per day for 2 months. Adaption training started at low speed (7 m/min) to ultimate speed (14 m/min) were performed for one week before mice were given high speed running experiments (14 m/min). Electric shock was on during the whole experiments. Mice were allowed to rest for 4 minutes in the middle of the experiments.

Micro-CT analysis

Dissected femurs in 70% ethanol were scanned by SKYSCAN 1272 3D X-ray microscope (Bruker). The femurs were scanned at the isotropic voxel sizes of 7 μm. The voltage and current were: 60 kV, 166 μA and 80 kV, 125 μA for 2- and 4-month-old mice, respectively. We set the bottom of the distal growth plate as start point and continued for 200 slices to measure trabecular bone parameters. 100 slices were chosen in the middle of diaphysis to measure cortical bone parameters. Bone structure parameters were interpreted according to previous guidance (Bouxsein et al., 2010).

CFU-F forming efficiency assay

Whole bone marrow cells were cultured in 6-well plates at densities ensuring that colonies would form at clonal density. The cultures were incubated at 37°C in a gas-tight chamber (Billups-Rothenberg) with 5% O_2 and 10% CO_2 for 7 days.

Bone fracture

Mice were anaesthetized by administered with 150 μL 7% chloral hydrate. One of the legs was shaved and scrubbed with 75% ethanol. One 25G needle was used to punch a hole into the marrow through the knee. A stainless steel wire (diameter less than 0.2 mm) was then inserted into intramedullary canal of the femur to stabilize the impending fracture. Three-point bending was performed to make the fracture. Buprenorphine was then used. Steel wire was taken out at 1 week after fracture. Mice were euthanized for analysis at 2 weeks or 8 weeks after fracture.

Lethal irradiation and bone marrow transplantation

Mice were given two doses of 540 rads by RS 2000 X-ray irradiator (Rad Source). At least 2 hours were needed between exposures. One million bone marrow cells were transplanted into irradiated mice in 24 hours to avoid hematopoietic failure. Mice were feed with antibiotic water (neomycin sulfate 1.11 g/l and polymixin B 0.121 g/l) for 14 days after transplantation.

QUANTIFICATION AND STATISTICAL ANALYSIS

Standard two-tailed Student's t tests and one-way ANOVA were used to analyze statistically significant values. Experiments were performed on at least 3 independent samples. P value less than 0.05 was considered as significant difference. Unless specifically pointed out, data were represented by mean ± SD.